High Quality Aluminium Doped Zinc Oxide Target Synthesis from Nanoparticulate Powder and Characterisation of Sputtered Thin Films

P. J. M. Isherwood[a*], N. Neves[b], J. W. Bowers[a], P. Newbatt[b] and J. M. Walls[a]

[a]*Centre for Renewable Energy Systems Technology, Loughborough University, Loughborough, Leicestershire, LE11 3TU, UK*

[b]*Innovnano, S. A., Rua Coimbra Inovação Parque, IParque Lote 13, 3040-570 Antanhol, Coimbra, Portugal*

[*]*Corresponding author. Tel: +44 (0)1509 635306. Email: P.J.M.Isherwood@lboro.ac.uk*

Abstract

Nanoparticulate aluminium-doped zinc oxide powder was synthesised through detonation and subsequent rapid quenching of metallic precursors. This technique allows for precise compositional control and rapid nanoparticle production. The resulting powder was used to form sputter targets, which were used to deposit thin films by radio frequency sputtering. These films show excellent sheet resistance and transmission values for a wide range of deposition temperatures. Crystal structure analysis shows that crystals in the target have a random orientation, whereas the crystals in the films grow perpendicular to the substrate surface and propagate preferentially along the (002) axis. Higher temperature deposition reduces crystal quality with a corresponding decrease in refractive index and an increase in sheet resistance. Films deposited between room temperature and 300 °C were found to have sheet resistances equivalent to or better than indium tin oxide films for a given average transmission value.

Keywords:

Aluminium-doped zinc oxide; AZO; ZnO:Al; Transparent conducting oxide; Sputter target synthesis; Compositional control; Nanoparticle synthesis

1. Introduction

Transparent conducting oxides (TCOs) are an unusual class of material with a wide range of uses. These include electronic screens and displays including touchscreen panels through to electrochromic windows, light-emitting diodes (LEDs) and solar cells [1], [2]. They are easily produced, and techniques such as chemical vapour deposition, magnetron sputtering and spray pyrolysis are regularly employed [3], [4]. The major concerns surrounding the metal oxide conductors are their brittleness and lack of flexibility, their inherent trade-off between transparency and conductivity [4], [5] and in a few cases cost, rarity and environmental issues associated with obtaining the raw materials [3], [4]. Despite these concerns, doped metal oxides are still the dominant type of transparent conductor, largely because of their good electrical properties, ease of formation and deposition and their relatively good chemical and thermal stability [6]. At present the most commonly used TCO is tin-doped indium oxide (indium tin oxide, or ITO) [1], but due to concerns over supply and cost of indium there has recently been an increasing interest in alternatives [7]. Aluminium-doped zinc oxide (AZO) is another commonly used TCO and is a cheaper alternative to ITO [7], [8].

In order to compete with ITO, alternatives must have as good or better electrical and optical properties. This means an average visible light (400 – 800 nm) transmission of around 80 %, and sheet resistances of 20 Ω/sq or less [9]. The best quality ITO films are usually deposited at elevated temperatures, which can cause serious problems for any temperature-sensitive technology such as organic solar cells and

LEDs [9]. Materials that can achieve similar transmission and sheet resistance values at lower deposition temperatures are therefore of significant interest.

The electrical and optical properties of sputtered thin films depend not only on the deposition parameters but also on the characteristics of the sputter target. In particular, grain size, density, oxygen content and homogeneity play an important role in the determination of target quality [10]–[14]. Innovonano S.A. has developed a patented nanoparticle-based route for the synthesis of AZO powders [15]. The following is a description and analysis of the material synthesis technique and characterisation of films sputtered from targets formed using this material.

2. Experimental details

2.1. Powder synthesis and target preparation

A pyrolysis production method was used to synthesize AZO nanostructured powder containing 0.5 wt. % Al dopant [15]. Nanoparticulate powder was synthesised by detonation of an emulsion containing metallic Zn and Al precursors in the same concentrations as the desired material composition (Fig. 1).

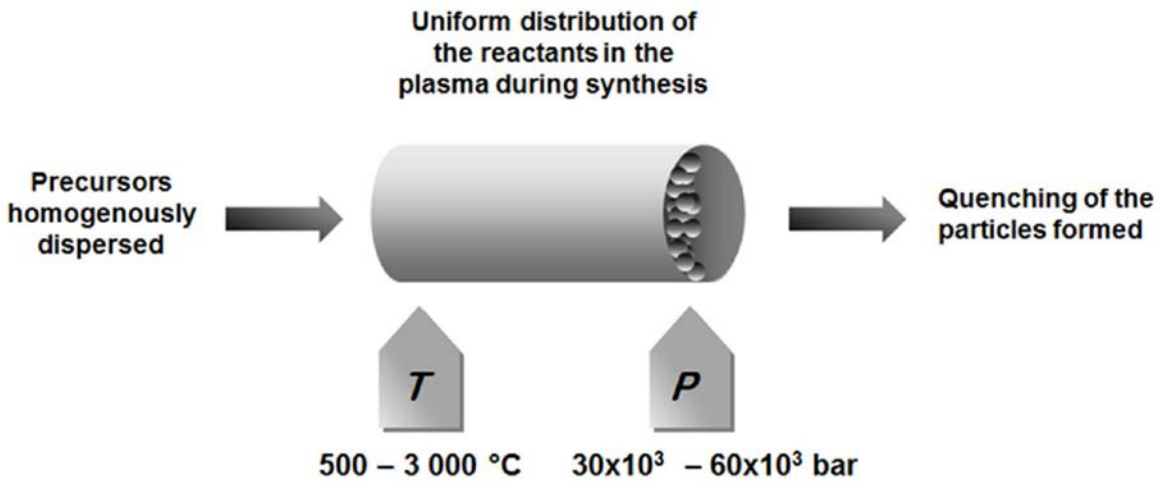

Figure 1: Synthesis method for the formation of AZO nanostructured powder

This method combines high pressures (>1000 MPa), high temperatures (500 – 3000 ^{o}C) and ultrafast quenching (10^{8} ^{o}C/s to 10^{9} ^{o}C/s). Powder crystal size is determined by the precise conditions used. The resulting material shows a structure composed of both individual and agglomerated nanoparticles (Fig. 2). Subsequent to formation, the powder was disaggregated in order to improve sinterability [8].

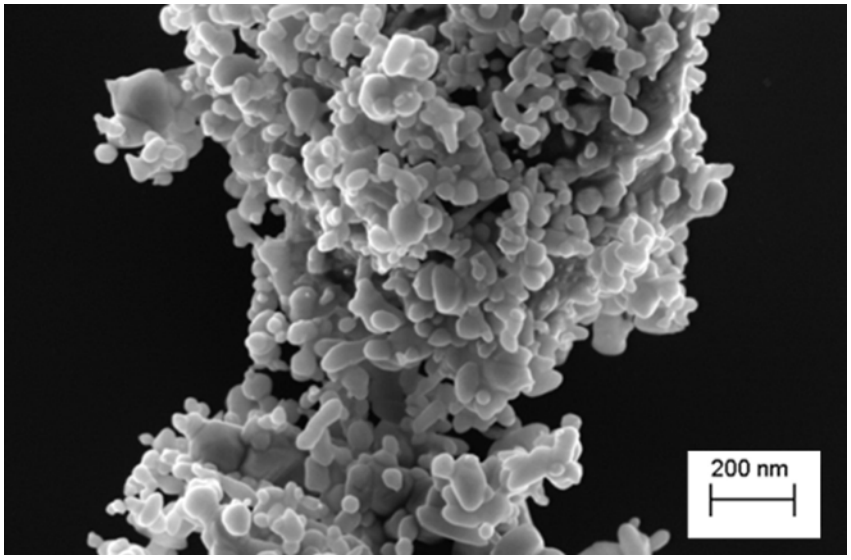

Figure 2: SEM image of the agglomerated AZO powder. Particles are approximately 20 – 40 nm across

Particle size distribution was measured using a CPS Disc Centrifuge (Model DC 20000, CPS Instrument Inc). A Quantachrome Nova 1000E Series equipment using helium as the carrier gas was used to determine the powder specific surface area. Crystal structure was measured using a Bruker D8 Advance X-ray diffractometer equipped with a Cu-K_{α} X-ray source. Scanning electron microscopy (SEM) was performed using a Zeiss Auriga CrossBeam scanning electron microscope equipped with a focused ion beam (FIB). Aperture size was 60 µm and the operating voltage was 5 kV. Transmission electron microscopy (TEM) was performed using an FEI Tecnai F20 field emission gun transmission electron microscope. TEM images were taken using a bright field detector at 200kV. TEM samples were prepared by FIB

milling using a dual beam FEI Nova 600 Nanolab SEM. A standard in-situ lift-out method was used to prepare cross-sectional samples. A platinum over-layer was deposited to define the sample surface and to homogenize the final sample thinning. Samples were thinned to 75 nm. The sputter target was prepared by hot-pressing in an argon atmosphere using an HPW 315/400-2200-1000. Sintering took place under a constant pressure of 50 MPa with a heating / cooling rate of 10 ºC/min and a holding time of 60 mins at 1025 ºC. The final density of the target was measured using the liquid displacement technique with distilled water. An image analyzer program was used to calculate the mean grain size of the sintered sample. Target electrical properties were measured using a Biorad HL 5500 Hall Effect device at room temperature using the van der Pauw configuration.

2.2. Film deposition and characterisation

AZO was sputtered onto 50 mm by 50 mm soda-lime glass slides using the AZO ceramic target. Films were deposited using an AJA International Orion 8HV sputter coater with an AJA 600 series RF power supply. Deposition conditions were kept at 180 Watts power (3.95 Watts/cm^2) with no oxygen input, 1 mTorr pressure (0.133 Pa) and 5 SCCM (8.33 x 10^{-8} m^3/s) of argon, whilst the temperature and deposition time were varied. Films were deposited over one, two and three hours, and the substrate temperatures used were room temperature, 100, 150, 200, 300 and 450 ºC. Each deposition temperature was used for each of the three deposition times. A second set of films was deposited from a commercially available non-nanoparticulate target for comparison. These films were deposited at 150 ºC. This temperature was chosen as it was found to give the best overall performance.

Film optical and electrical characterisation were carried out using an Ambios XP2 stylus profilometer to measure thickness, a Varian Cary 5000 spectrophotometer for

transmission spectra and an Ecopia HMS 3000 Hall effect system for mobility, resistivity and carrier concentration measurements. Film roughness measurements were taken using a Taylor-Hobson Sunstar-HD Coherence Correlation Interferometer (CCI), and refractive index and extinction coefficient measurements were taken using a Horriba iHR320 ellipsometer. A four-point probe was used to measure sheet resistance. Structural characterisation was carried out using both scanning and transmission electron microscopes. SEM was conducted using a Carl Zeiss (Leo) 1530 VP field emission gun scanning electron microscope. Aperture size was 30 μm and the operating voltage was 5 kV. TEM was conducted using an FEI Tecnai F20 field emission gun transmission electron microscope, equipped with a bright field detector and at an operating voltage of 200 kV. TEM samples were prepared by the same method as described for the sputter target characterisation. X-ray diffraction (XRD) was performed using a Brucker D2-phaser desktop X-ray diffractometer equipped with a Cu-K_α X-ray source and Lynxeye^{TM} detector. The beam slit was 1 mm wide, and the antiscatter plate was positioned 3 mm above the sample. The sample was rotated at 15 revolutions per minute. Structural characterisation was performed on selected samples only.

3. Results and Discussion

3.1. Powder and sputter target characterisation

The powder particle size distribution reveals two different groups of particles. The powder is largely composed of nanoparticles (~ 30 % wt. fraction) of about 40 nm in size (Fig. 2). Some larger particles are also present (~70 % wt. fraction) which exhibit random morphology. These are composed of coalesced nanoparticles and some

fragmented particles. Figure 3 shows the XRD pattern of the powder (a) and sintered target (b).

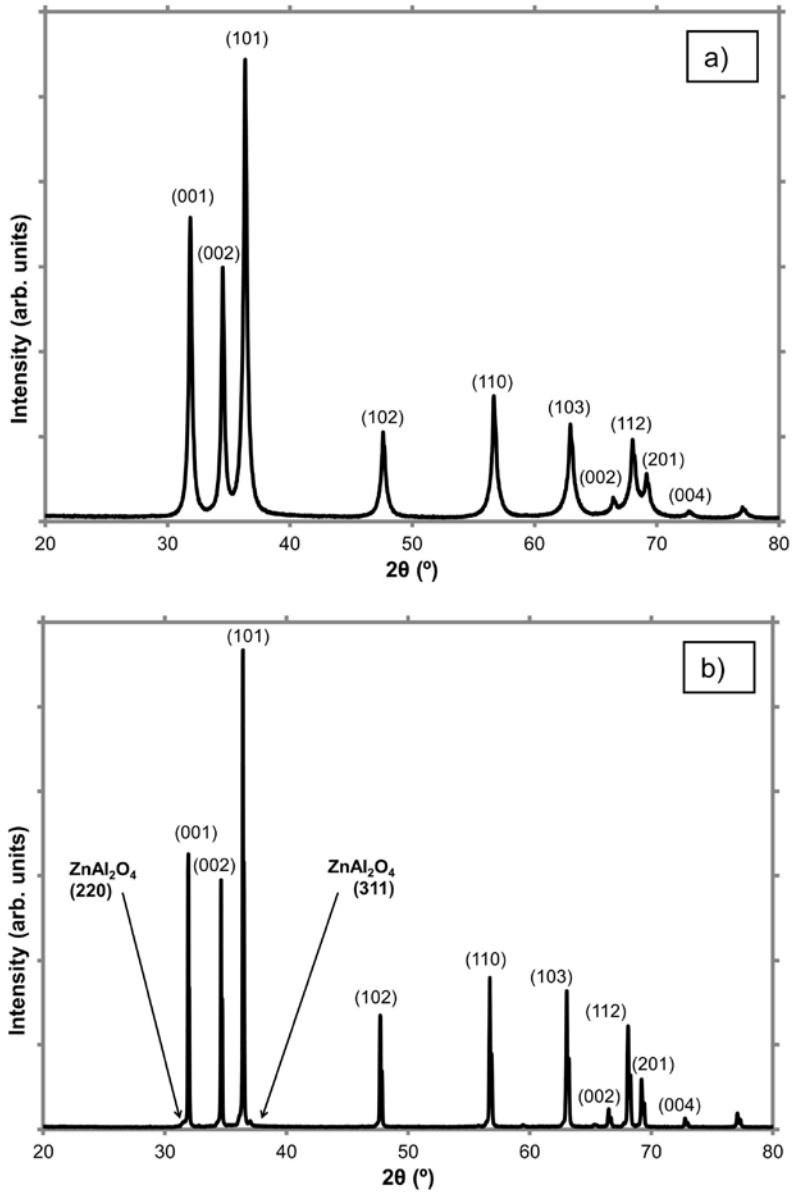

Figure 3: XRD pattern of AZO powder (a) and AZO sintered target (b)

Using the Scherrer equation [16], crystallite size was found to be 19 nm, in line with the broad diffraction curve and the high specific surface area obtained (12.55 $m^2.g^{-1}$). Only the wurtzite phase was identified in the powder. XRD performed on the sintered target revealed that whilst wurtzite is the primary phase, a minor secondary

phase, $ZnAl_2O_4$ (ghanite) is also present. This is typically seen when Al concentrations above the solid solubility limit are used [17].

An important aspect of the synthesis technique used is that it allows for rapid and simple alteration of the composition of the powder, and therefore of the sputter target, with the aluminium dopant being uniformly incorporated into the zinc oxide structure. This is in contrast to more standard target synthesis techniques (eg [18]), and means that both nanoparticulate powders and sputter targets can be tailored to suit a wide range of uses and requirements.

The high sinterability of the AZO powder [11] allowed us to achieve a high density target (>98 % of theoretical density, (5.61 $g.cm^{-3}$)). TEM and SEM images of the AZO target show that it is composed of small, regular crystals of between 0.5 µm and 1.0 µm (Fig. 4). The consistent crystal size and lack of Al_2O_3 peaks in the XRD pattern indicate that the target material is highly homogenous.

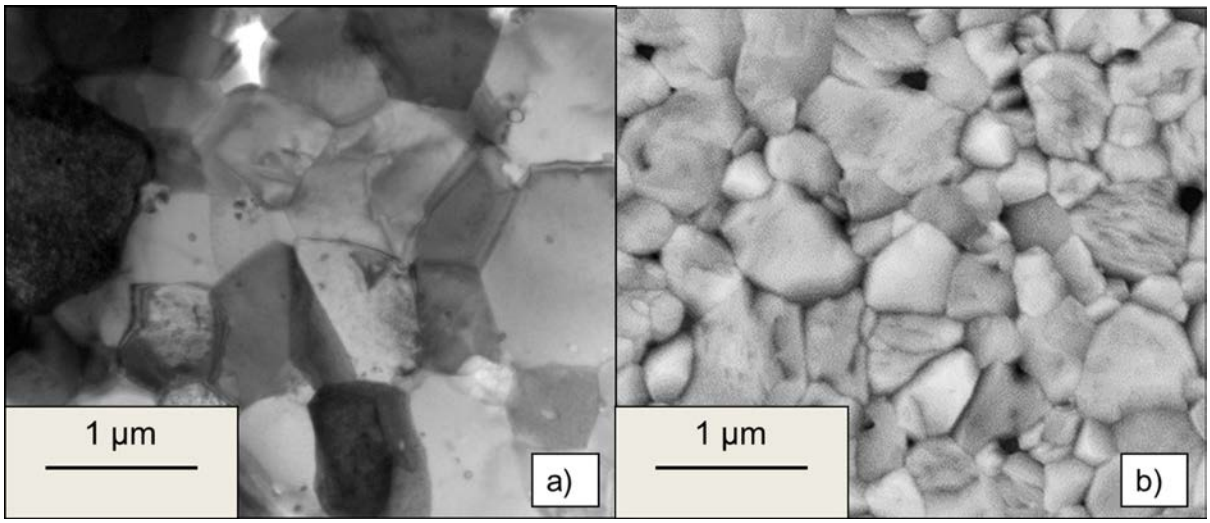

Figure 4: TEM (a) and SEM (b) images of the AZO target material sintered by hot-pressing at 1025 °C for 1 hour

The target has an electrical resistivity of 4.01×10^{-4} Ω.cm, with a carrier concentration of 4.03×10^{20} cm^{-3} and a mobility of 38.67 cm^2/Vs. These values are in good

agreement with those obtained by others [10]–[12] and demonstrate that this technique can be used to produce high quality ceramic sputtering targets [10]–[13], [19].

3.2. Film deposition and characterisation

The deposition rate was found to be approximately 5.5 nm/minute, with film thicknesses of 330 nm after 1 hour, 660 nm after 2 hours and 1 μm after 3 hours. This is slow when compared to alternative sputter deposition methods such as direct current (DC) and pulsed DC systems, and is a recognised issue with RF sputtering (eg, [20]). It is likely that the use of DC or pulsed DC power rather than RF would significantly increase the deposition rate, which would make this material more commercially attractive.

Transmission spectra for each film show that as the film thickness is increased, transmission across both the visible and infrared ranges drops, with the highest losses being in the infra-red. This decrease appears greatest between the 330 nm and 660 nm thick films (Fig. 5). Transmission in the infrared appears highest for low temperature and high temperature (particularly 450 ºC) depositions, with films deposited between 100 and 200 ºC showing marginally better transmissions in the visible range.

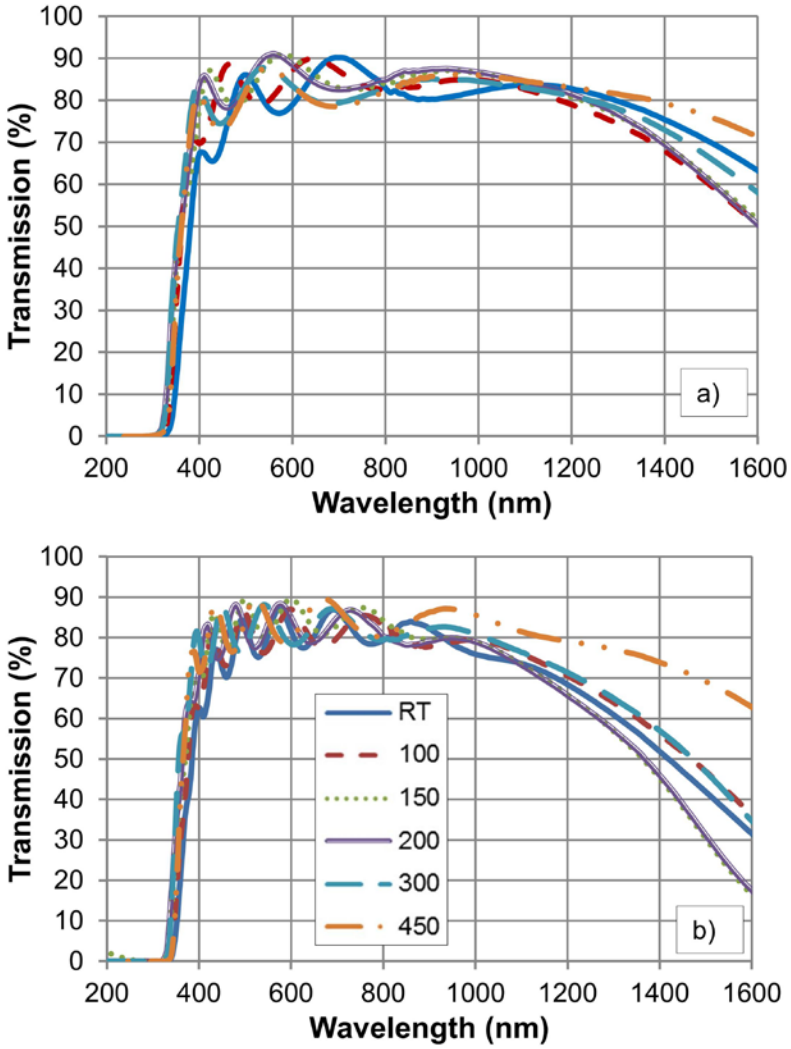

Figure 5: Transmission data for films of (a) 330 nm and (b) 660 nm thickness.

The sheet resistance varies from 35 Ω/sq to around 3.1 Ω/sq, with specific values depending on both deposition temperature and film thickness. Although less apparent for thinner films, there is a trend for the sheet resistance to decrease slightly towards temperatures of 100ºC to 200 ºC before rising slightly to 300 ºC and then more rapidly beyond that (Fig. 6).

Overall, the carrier concentration increases with increasing temperature up to 300 ºC, which begins to plateau above 200 ºC. The carrier concentration drops significantly with a further increase in temperature from 300 to 450 ºC. The mobility doesn't change dramatically with increasing temperature, with films typically showing

mobilities of between 20 and 40 $cm^2/V.s$ (Fig. 7). The only thickness which demonstrates a clear trend is 1 μm, where mobility increases up to a deposition temperature of 150 °C, before dropping off at higher temperatures. The film resistivity shows an increase from 300 to 450 ºC (Fig. 8).

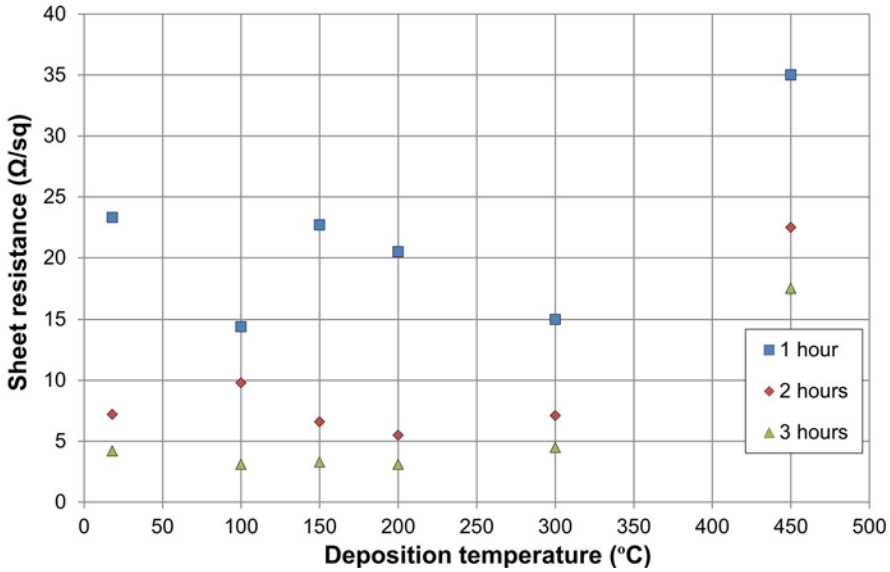

Figure 6: Sheet resistance dependence on deposition temperature. There is an obvious increase in sheet resistance for all thicknesses between 300 ºC and 450 ºC

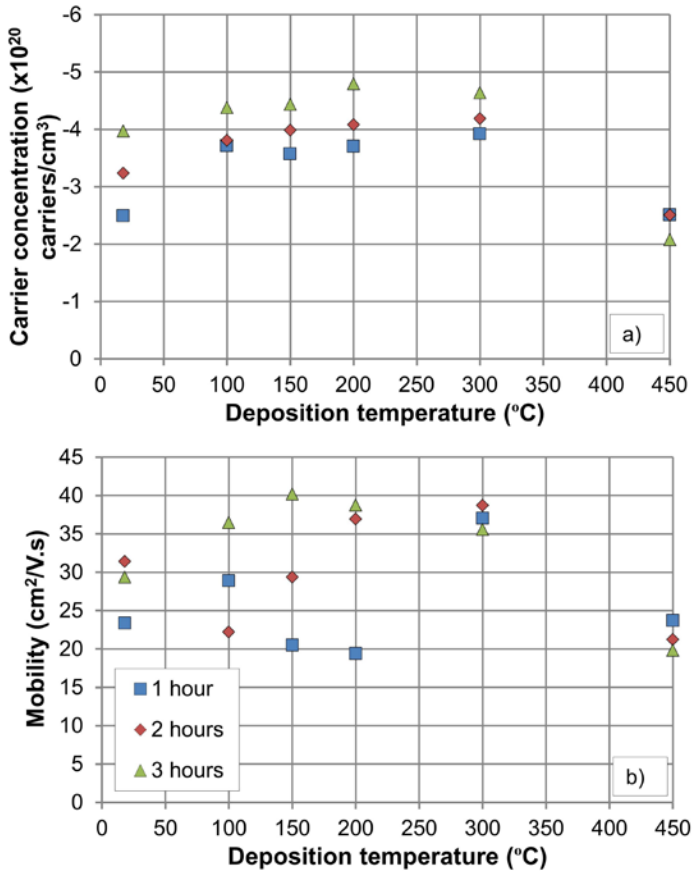

Figure 7: Carrier concentration (a) and mobility (b) dependence on deposition temperature. Carrier concentration was found to increase up to 300 ºC, then drop significantly as the temperature increased to 450 ºC. A similar trend is seen for mobility in thicker films, although it is less apparent for the 330 nm films

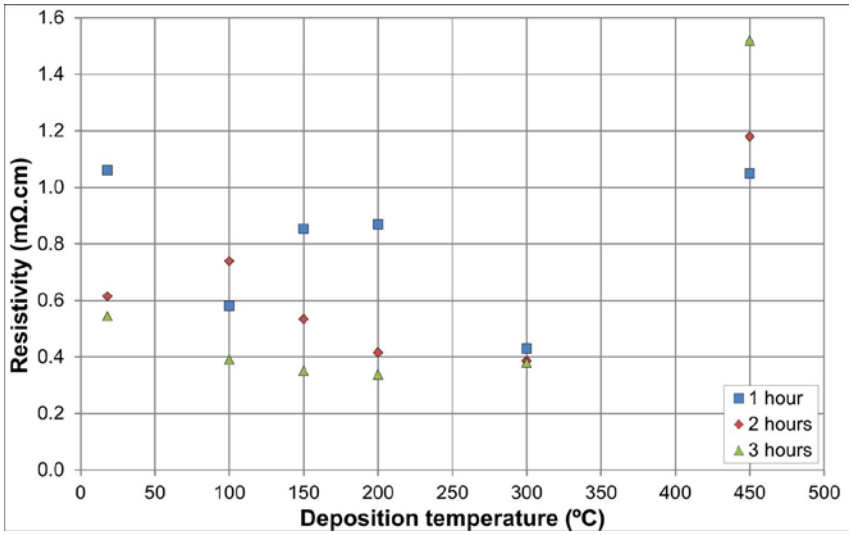

Figure 8: Resistivity against deposition temperature. There is a slight overall decrease in resistivity up to 300 ºC, with a marked increase at 450 ºC

SEM images show that the films are largely crystalline, with crystal size increasing significantly with increasing temperature up to 150 ºC. Further increasing the temperature reduces crystallinity dramatically, with films deposited at 300 ºC and above exhibiting much smaller crystals and an apparent increase in film surface defects (Fig. 9).

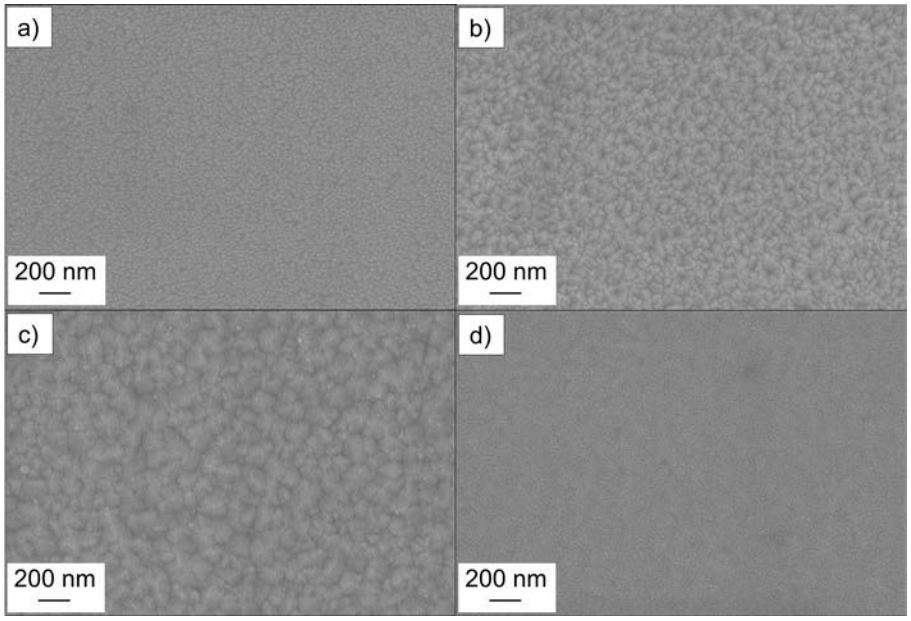

Figure 9: SEM images of samples deposited for two hours (660 nm thickness) at room temperature (a), 100ºC (b), 150ºC (c) and 300 ºC (d). All images were taken at 100,000 times magnification

TEM images show that films deposited at higher temperatures retain a degree of crystallinity, but the individual crystals are smaller and show a high level of defects when compared to films deposited at lower temperatures (Fig. 10). The crystals for all films are approximately perpendicular to the substrate surface, and appear columnar. XRD analysis of the films showed that at all temperatures, the predominant signal was from the (002) plane, with a slight secondary peak from the (004) plane (Fig. 11).

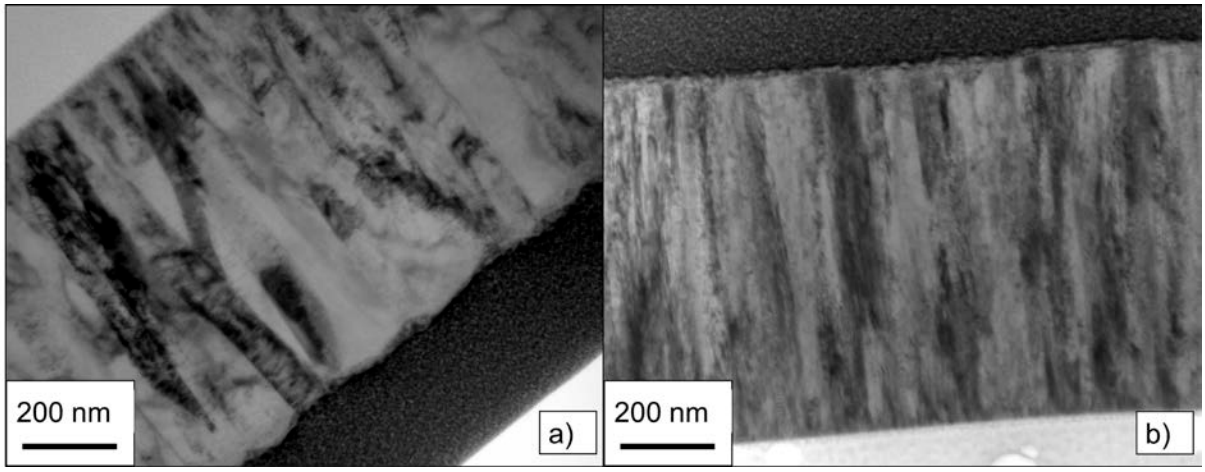

Figure 10: TEM images of films deposited at 150 ºC (a) and 450 ºC (b). While b) shows a crystalline structure, the crystals are both smaller and less well-formed than those in a).

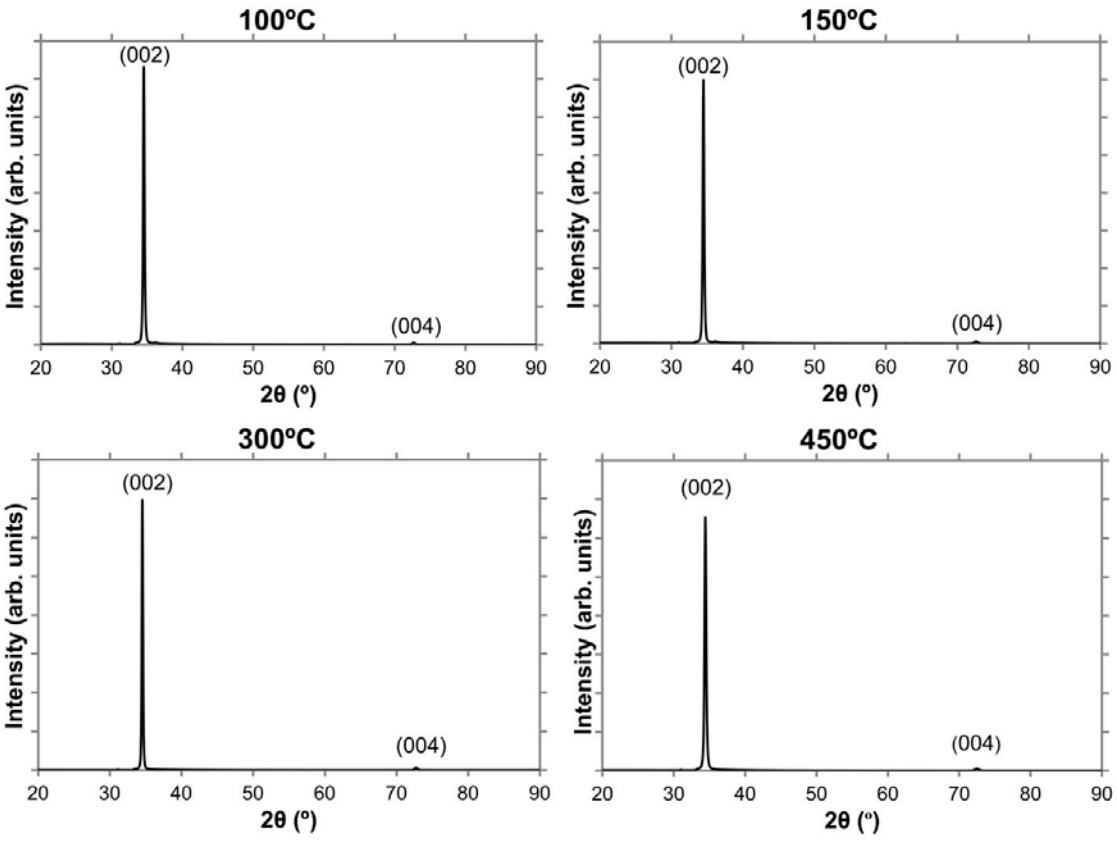

Figure 11: XRD patterns for films deposited at 100 ºC, 150 ºC, 300 ºC and 450 ºC. All show a prominent (002) peak and a small secondary (004) peak

Coherence correlation interferometry measurements show that the films are all very smooth, with root mean square surface roughness of between 1 and 3nm.

The refractive index was found to be 1.9 +/- 0.04 at 550 nm for films deposited at temperatures up to 200 ºC. This is in good agreement with literature values (eg, [21], [22]). For the 300 and 450 ºC films, the refractive index was found to be significantly lower, at 1.6 +/- 0.04.

Overall, transmission in the visible range (400 – 800 nm) for these films is good, being at or above an average of 78 % for all temperatures and thicknesses. The drop in transmission in the infrared shown by all films is due to their having a high charge carrier concentration [4]. The thicker films display lower infrared transmission values due to higher carrier concentrations. There are some specific applications where this could be a problem, notably certain types of photovoltaic cell such as tandem and multijunction devices where infrared light adds significantly to the photocurrent of the bottom absorber layers [23]. However for the vast majority of PV applications it is unlikely to be a problem as the transmission is consistently above 70 % as far as 1200 nm, which is into the infra-red and equates to a band gap of ~1 eV. The reason for the slight reduction in transmission in the visible range for both high and low temperature films is less obvious.

The variation in sheet resistance is unusual because of the sudden increase with temperatures above 300 ºC. This behaviour has been observed by other groups [24], [25], and correlates with the measured film refractive indices. It is possible that at higher substrate temperatures films are either losing zinc (via re-evaporation of as-deposited zinc species), or the aluminium is migrating to the grain boundaries where it forms aluminium oxide rather than continuing to act as a dopant. Either effect would explain the drop in carrier concentration and hence the increased resistivity and infrared transmission. The highest temperature films appeared to be the least crystalline and contained the highest levels of defects suggesting that

higher temperatures and hence increased system energy are the cause of the reduced conductivity. However, as the 300 ºC films still demonstrated a good sheet resistance despite showing reduced crystal quality it is possible that the two are not directly related. Films deposited at lower temperatures were all found to be fully crystalline, with crystal size increasing dramatically with increased temperature and deposition time. The lack of variation in sheet resistance and refractive index for lower temperature films indicates that whilst crystal size may have an impact on the optical and electrical properties, it is not the limiting factor. The most plausible explanations are either that crystal quality is of greater importance, or that the change in crystal quality is coincidental, and some concurrent change in either the doping level or film stoichiometry is the key. Further work would be required to verify either hypothesis. The increase in resistivity with increased deposition temperatures is commonly observed in AZO films (eg, [24], [25], [26]), which implies that it is a fundamental property of the material. This means that this material is not suitable for use in higher temperature processes.

For a given average transmission value, the AZO samples described in this study deposited at temperatures of up to 300 ºC show equivalent (and often lower) sheet resistances to those published for ITO (eg, [27]). This demonstrates that this material is an ideal alternative to ITO, especially when material scarcity and cost issues are taken into account. In particular, films deposited at room temperature show excellent transmission and sheet resistances, meaning that this material is ideal for use in temperature sensitive applications such as organic electronics.

AZO films deposited from this target show equivalent and in some instances improved characteristics when compared to films deposited from a standard commercially available non-nanoparticulate target. Transmission in the visible range

was found to be virtually identical, although lower temperature films demonstrated a greater drop in transmission in the infrared than films from the commercial target. Carrier concentration was found to be around three times that of films deposited from the commercial target, which is almost certainly the cause of the reduced infrared transmission. Mobility was found to be the same at around 40 – 45 cm^2/V.s, and resistivity was found to be approximately a third that shown by films from the commercial target. The deposition rate was identical for both targets.

XRD analysis showed that whilst both compressed and powder target material exhibited the complete range of ZnO peaks, the sputtered films had a single prominent peak from the (002) plane, with a very minor secondary (004) signal. This is something that other groups have noticed (eg, [10]), and indicates that sputtered ZnO grows in the wurtzite (zincite) phase and preferentially along the 'c' axis. TEM images confirm this, showing that crystals grow perpendicular to the substrate surface in columns. The sputtered films also showed no evidence of $ZnAl_2O_4$ formation, despite trace amounts of this showing up in XRD analysis of the target material.

CCI analysis showed that roughness changed remarkably little, with RMS values ranging from 1 to 3 nm. Overall, roughness was found to change in line with the observed changes in crystallinity. Finely crystalline films grown at room temperature were the smoothest, with roughness increasing as the crystal size increased, up to 200 ºC. At higher temperatures roughness was found to decrease as crystal size and quality reduced.

4. Conclusions

AZO sputtering targets were produced from nanoparticulate AZO powder. The synthesis technique allows for simple tailoring of the powder and hence target composition. The target material was found to show random crystal orientation, with a large range of different crystal sizes. XRD analysis indicated that crystals had the wurtzite structure. A small degree of $ZnAl_2O_4$ was found to have formed during the manufacturing process, however this was not seen in the as-deposited films.

SEM, TEM and XRD analysis of the films all show that crystallinity increases with increasing temperature up to 300 ^oC. Above this, crystal size and quality are reduced significantly. Crystals were found to grow preferentially along the (002) axis, propagating perpendicular to the substrate surface. Crystal size and quality is reflected in the carrier concentration, mobility and sheet resistance data, with sheet resistances decreasing slightly with increasing temperatures and crystal size. Above 300 ^oC, sheet resistance increases dramatically. There are various possible explanations for this increase, and work to establish the cause is ongoing. It is probable that the degradation in crystal quality and increase in resistivity are directly linked, and are most likely caused by the same effect.

Consistent high quality room temperature films with good transmission values and low sheet resistances demonstrate that this material is ideally suited for use in temperature-sensitive applications. Compared with published ITO data, AZO films were found to display equivalent sheet resistances for a given average transmission value. This demonstrates that AZO synthesised using the conditions described is an ideal alternative to ITO.

Acknowledgements

The authors from Loughborough University would like to acknowledge funding for the work through the EPSRC Supergen Supersolar Hub. They would also like to acknowledge the invaluable help and support of Biancamaria Maniscalco and Fabiana Lisco for assistance with CCI and ellipsometry measurements, and Ali Abbas for assistance with structural characterisation.

References

[1] B. G. Lewis and D. C. Paine, Applications and Processing of Transparent Conducting Oxides, MRS Bull. 25, 08 (2000), 22–27.

[2] S. Fernández and F. B. Naranjo, Optimization of aluminum-doped zinc oxide films deposited at low temperature by radio-frequency sputtering on flexible substrates for solar cell applications, Sol. Energy Mater. Sol. Cells 94, 2 (2010), 157–163

[3] D. S. Ginley, Nanoparticle Derived Contacts for Photovoltaic Cells, Electrochem. Soc. Proc. 99, 11 (1999), 103–110

[4] D. S. Ginley, H. Hosono, and D. C. Paine, Eds., Handbook of Transparent Conductors. London: Springer, 2010, p. 533.

[5] J.-Y. Lee, S. T. Connor, Y. Cui, and P. Peumans, Solution-processed metal nanowire mesh transparent electrodes, Nano Lett. 8, 2 (2008), 689–92

[6] R. G. Gordon, Criteria for Choosing Transparent Conductors, MRS Bull. 25, 08 (2000), 52–57

[7] S. Suzuki, T. Miyata, M. Ishii, and T. Minami, Transparent conducting V-co-doped AZO thin films prepared by magnetron sputtering, Thin Solid Films 434 (2003), 14–19

[8] B. Thestrup and J. Schou, Transparent conducting AZO and ITO films produced by pulsed laser ablation at 355 nm, Appl. Phys. A 69 (1999), 807–810

[9] T. Gorjanc, D. Leong, C. Py, and D. Roth, Room temperature deposition of ITO using r.f. magnetron sputtering, Thin Solid Films 413 (2002), 181–185

[10] T. Minami, J. Oda, J. Nomoto, and T. Miyata, Effect of target properties on transparent conducting impurity-doped ZnO thin films deposited by DC magnetron sputtering, Thin Solid Films 519 (2010), 385–390

[11] N. Neves, R. Barros, E. Antunes, J. Calado, E. Fortunato, R. Martins, and I. Ferreira, Aluminum doped zinc oxide sputtering targets obtained from nanostructured powders: Processing and application, J. Eur. Ceram. Soc. 32, 16 (2012), 4381–4391

[12] H. S. Huang, H. C. Tung, C. H. Chiu, I. T. Hong, R. Z. Chen, J. T. Chang, and H. K. Lin, Highly conductive alumina-added ZnO ceramic target prepared by reduction sintering and its effects on the properties of deposited thin films by direct current magnetron sputtering, Thin Solid Films 518 (2010), 6071–6075

[13] G. Falk, Sintering of Transparent Conductive Oxides : From Oxide Ceramic Powders to Advanced Optoelectronic Materials, in: A. Lakshmanan, Ed., Sintering of Ceramics - New Emerging Techniques, Rijeka, 2012, pp. 587 – 609.

[14] G. Zhu, L. Zhi, H. Yang, H. Xu, and A. Yu, Effect of Target Density on Microstructural, Electrical, and Optical Properties of Indium Tin Oxide Thin Films, J. Electron. Mater. 41, 9 (2012), 2376–2379

[15] J. M. Calado Da Silva and E. M. D. S. Antunes, Nanometric-Sized Ceramic Materials, Process for their Synthesis and Uses Thereof, US patent 20110129670A12011.

[16] A. L. Patterson, The Scherrer Formula for X-Ray Particle Size Determination, Phys. Rev. 56 (1939), 978–982

[17] K. Shirouzu, T. Kawamoto, N. Enomoto, and J. Hojo, Dissolution Behavior of Al and Formation Process of ZnAl2O4 Phases in Al2O3-Doped ZnO Sintered Bodies, Jpn. J. Appl. Phys. 49, 1 (2010), 010201 – 010203

[18] B. L. Gehman, S. Jonsson, T. Rudolph, M. Scherer, M. Weigert, and R. Werner, Influence of manufacturing process of indium tin oxide sputtering targets on sputtering behavior, Thin Solid Films, 220 (1992), 333–336

[19] M.-W. Wu, D.-S. Liu, and Y.-H. Su, The densification, microstructure, and electrical properties of aluminum-doped zinc oxide sputtering target for transparent conductive oxide film, J. Eur. Ceram. Soc. 32, 12 (2012), 3265–3275

[20] K. Ellmer and R. Wendt, D.C. and R.F. (reactive) magnetron sputtering of ZnO:Al films from metallic and ceramic targets: a comparative study, Surf. Coatings Technol. 93, 1 (1997), 21–26

[21] W. Yang, Z. Liu, D.-L. Peng, F. Zhang, H. Huang, Y. Xie, and Z. Wu, Room-temperature deposition of transparent conducting Al-doped ZnO films by RF magnetron sputtering method, Appl. Surf. Sci. 255, 11 (2009), 5669–5673

[22] J. W. Leem and J. S. Yu, Structural, optical, and electrical properties of AZO films by tilted angle sputtering method, Thin Solid Films 518 (2010), 6285–6288

[23] S. Wenger, S. Seyrling, A. N. Tiwari, and M. Grätzel, Fabrication and performance of a monolithic dye-sensitized TiO2/Cu(In,Ga)Se2 thin film tandem solar cell, Appl. Phys. Lett. 94, 17 (2009), 173508-1 - 173508-3.

[24] J. H. Park, J. M. Shin, S.-Y. Cha, J. W. Park, S.-Y. Jeong, H. K. Pak, and C.-R. Cho, Deposition-Temperature Effects on AZO Thin Films Prepared by RF Magnetron Sputtering and Their Physical Properties, J. Korean Phys. Soc. 49 (2006), 584–588

[25] J. F. Chang and M. H. Hon, The effect of deposition temperature on the properties of Al-doped zinc oxide thin films, Thin Solid Films 386 (2001), 79–86

[26] F.-J. Haug, Z. Geller, H. Zogg, A. N. Tiwari, and C. Vignali, Influence of deposition conditions on the thermal stability of ZnO:Al films grown by rf magnetron sputtering, J. Vac. Sci. Technol. A 19, 1 (2001), 171-174.

[27] C. Guillén and J. Herrero, Comparison study of ITO thin films deposited by sputtering at room temperature onto polymer and glass substrates, Thin Solid Films 480–481 (2005), 129–132